Ocean wind fields and their variability derived from SAR

J. Horstmann[1], Wolfgang Koch[1], S. Lehner[2] & W. Rosenthal[1]

[1]GKSS Forschungszentrum Geesthacht
Max-Planck-Str. D-21502 Geesthacht, Germany
phone: +49-4152-87.1567 - fax: +49-4152-87.1565 - e-mail: Horstmann@gkss.de

[2]Deutsche Forschungsanstalt für Luft- und Raumfahrt e.V., DFD
D-82230 Wessling, Germany
phone: +49-8153-28.2828 - fax: +49-8153-28.1445 - e-mail: Susanne.Lehner@dlr.de

The Synthetic Aperture Radar (SAR) aboard the European Space Agency's remote-sensing satellites (ERS-1 and ERS-2) acquires images that can be used to derive wind fields over the ocean surface. The SAR measures the backscatter, which is a measure of the roughness of the ocean surface. The roughness is strongly influenced by the local wind field so that the radar backscatter can be used to measure the wind. For the derivation of the wind field from SAR images the empirical C-band models are applied, which were originally developed for the wind scatterometer (SCAT), that operates at the same wavelength as the SAR. Scenes at different geographical locations and under different meteorological and oceanographical conditions were selected to test the applicability of the ERS SAR for retrieving wind fields over the ocean. Especially in coastal regions, the SAR-derived mesoscale wind fields give a lot of additional information. As an example, an ERS SAR-retrieved wind field is compared to ground truth measurements and to the results of a mesoscale atmospheric model.

Introduction

Mesoscale wind fields over the ocean surface are of great interest for studying processes in the boundary layer and for obtaining a better understanding of coastal processes. Spatial covering wind fields are frequently derived from space-borne scatterometers (SCAT). The SCAT and the Synthetic Aperture Radar (SAR) aboard the European remote-sensing satellites ERS-1 and ERS-2 operate both at 5.3 GHz (C-band) at moderate incidence angles between 18° and 59°. For these incidence angles, the backscatter signal of the rough ocean surface is primarily caused by the short surface gravity waves, which are in resonance with the incident radiation of the sensor. For incidence angles of ERS SARs, between 20° and 26°, the range of scattering wavelengths extends from 8.2 to 6.5 cm. These waves are strongly influenced by the local wind field and allow the backscatter to be a measure of the wind.

For several applications, especially in coastal regions the spatial resolution of the ERS SCAT (45 · 45 km, with a swath width of 500 km) is insufficient. The ERS SAR's high resolution of about 25 · 25 m and swath width of 100 km offer a unique opportunity to derive mesoscale wind fields over the ocean surface. A lot of effort has been

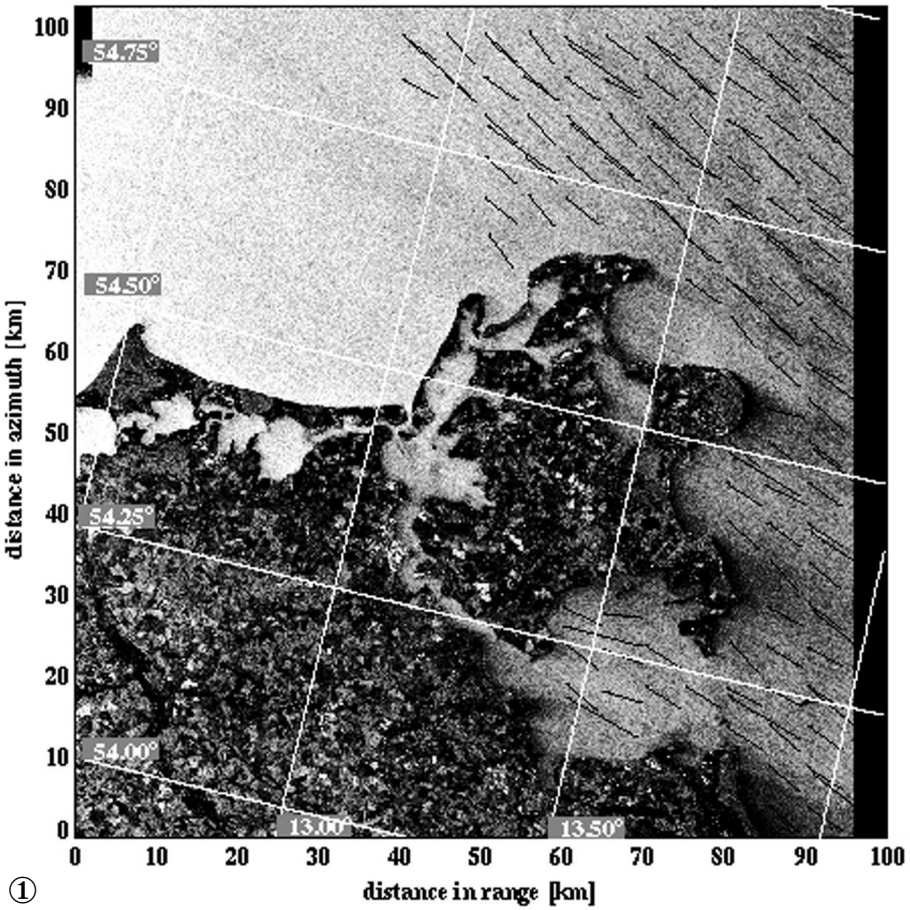

①

SAR image of the island Rügen at the Baltic coast of Germany, taken on 12 August 1991, at 21:07 UTC from ERS-1. The solid black lines in the right part of the image give the orientation of the visible wind streaks from which the wind direction was computed for 10 × 10 km thick lines and 5 × 5 km thin lines. The 180° ambiguity could be removed due to the shadowing of the coast.

invested in the derivation of wind speed from SAR images, [see e.g. *Alpers et al.* 1994, *Chapron et al.* 1994, *Scoon et al.* 1996, and *Horstmann* 1997]. Furthermore, the derivation of wind direction in addition to the wind speed was derived from SAR images, [see e.g. *Wakerman et al.* 1996, *Vachon et al.* 1996, *Korsbakken et al.* 1996, and *Lehner et al.* 1998]. In the first part of this article the method to derive wind speeds and wind directions from ERS SAR images is introduced. In the second part an example at the German coast of the Baltic Sea is given and compared to a mesoscale numerical model. Finally, the ERS SAR-derived wind fields are applied to investigate the spatial variability of the wind field.

Wind from SAR

For derivation of the wind speed from ERS-1 and 2 SAR images the empirical C-band models CMOD4 [*Stoffelen & Anderson* 1997] or CMOD IFR2 [*Quilfen & Bentamy* 1994] can be used. Both models were originally developed for the SCAT aboard ERS-1 and 2. These models require input of the normalised radar cross section (NRCS), the incidence angle of the radar beam, and the wind direction. The NRCS and the incidence angle can be derived in a straightforward manner from the ERS SAR data. Due to the fact that small changes in NRCS result in large changes in wind speed, the SAR images have to be calibrated as accurately as possible.

Details about the calibration are given in *Laur et al.* 1997. The wind direction can be derived from ERS SAR images if wind streaks are present. Figure 1 shows an ERS-1 SAR image with clearly imaged wind streaks from which the wind direction is derived with an 180° ambiguity. In approximately 65% of the investigated SAR images, wind streaks are present from which the wind direction can be extracted. Shadowing of the wind field for instance due to the coastal topography removes the 180° ambiguity of wind direction. For derivation of the wind direction a 10 · 10 km sub-image is analysed with a two-dimensional fast Fourier transform (FFT). The results of one sub-image are plotted in Figure 2. The grey levels represent energies of the power spectrum which are plotted for wavelengths between 500 and 1500 m. The resulting wind direction (solid line) is perpendicular to the dashed line depicting the direction of peak power of wind streaks.

Comparison with a numerical model

For the study of coastal processes, high-resolution wave and current models are used which require detailed wind information to calculate hydrographic parameters. Therefore, it is important to test the capability of ERS

Power spectrum of an area in the open water north of Rügen. Wavelengths between 500 and 1500 m are taken for the estimation of wind direction. The main energy is along an orientation of 26° versus north; the resulting main wind direction is orientated perpendicular.

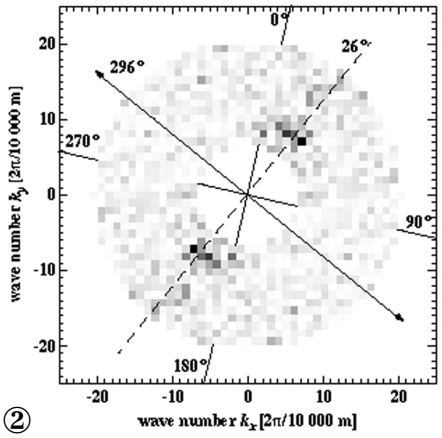

②

SAR to reproduce spatial variations of the wind field. Due to the complex topographic structure, the island Rügen near the German coastline at the Baltic Sea was chosen as a test site. The ERS-1 SAR image of this area is shown in Figure 1. For validation, the mesoscale atmospheric 'Geesthacht Simulation' model GESIMA, developed at GKSS Research Centre is used. It is a three-dimensional non-hydrostatic mesoscale model of atmospheric circulation [details are provided in *Kapitza and Eppel* 1992]. For this application, it was set up with 8 layers between 0 and 1500 m and a horizontal resolution of 1 · 1 km. The roughness length over the water surface is given according to Charnock's relation and over land from land use charts. For the upper boundary condition at 1500 m height, stationary wind speeds of 16 m/s coming from 306° were prescribed, and the model was run assuming neutral atmospheric stratification. The NRCS and incidence angles from the ERS-1 SAR image from 12 August 1991, at 21:07 UTC were computed with a horizontal resolution of 1 · 1 km. For the wind derivation a constant wind direction of 290° was assumed. Figure 3 shows the results of GESIMA and of the ERS SAR image using the CMOD4. The SAR image shows much finer detail in wind structure and a higher spatial variability than the modelled wind field. This is caused by the difference between the snapshot of a highly turbulent wind field from ERS SAR and the simulation with a mesoscale model assuming a stationary situation. On the ocean surface north of Rügen, the SAR image shows wind rolls from which the wind direction was derived. The GESIMA model cannot reproduce these features. This shows that the ERS SAR data give a lot of additional information on the turbulent structure of the atmosphere. East of the island of Rügen, the wind shadowing shows the same order of magnitude. The wind speed drops down to about 6 m/s behind the island, but picks up again toward the open ocean. The geometrical location of the wind shadowing in the ERS SAR and GESIMA data is slightly different, showing again that the results of GESIMA yield a much smoother solution than the distribution of wind speed in nature. Since the model has been run for stationary conditions, a full coincidence with the ERS SAR derived wind field cannot be expected.

Spatial wind variability

The wind fields from ERS SAR give a unique opportunity to investigate the variation of the wind field in space. In the conventional method using analysis of time series from a point measurement, Taylor's hypothesis is assumed. Taylor considers the turbulence to be frozen as it advects past the measuring sensor. Therefore, the wind speed can be used to translate turbulence measurements as a function of time to their corresponding measurements in space. The ERS SAR-derived wind fields are a snapshot of the surface wind field of an area of up to 100 · 100 km. Figure 4 shows an example of a SAR image from 1 December 1992 northwest of the Shetland Islands. There are range-travelling waves with approximately 300 m wavelengths visible in the complete ERS SAR image. The superimposed solid lines represent the wind directions computed from the imaged wind streaks. Due to shadowing off the coast of the Shetlands the 180° ambiguity could be removed. Using the mean wind direction, the wind speed was computed at a resolution of 100 · 100 m. This resulted in a mean wind speed of 14 m/s. The wind-speed spectrum was computed from the wind speeds with a two-dimensional FFT. To get an idea of the distribution of the spectral amplitude in wave number, the wind-speed spectrum was integrated over all directions and plotted in a double logarithmic plot (Fig. 5). The wave number and the corresponding wavelength are plotted versus the spectral density of the wind speed. Between wavelengths of 56 km and 2 km, the spectral density decreases. For lower wavelengths the spectral density begins to increase. This tendency was observed in several investigated SAR images. The slope of the spectra between 100 km and 2 km wavelengths varied between -1.1 and -1.6 while the slope below 2 km is approx. 1. The change of the spectral density in Figure 4 at wavelengths of approx. 300 m is due to the sea-state. Spectral density decreases with increasing wavelengths are a commonly observed phenomenon in the troposphere [*Gage & Nastrom* 1986] and at lower scales in the boundary layer [*Kaimal et al.* 1972]. Speckle effects dominate for resolutions below 2 · 2 km. Due to the distribution, the slope for wavelengths below ~2 km is approx. 1 and dominates the wind variability.

Wind speeds computed by the Geesthacht simulation model of the atmosphere (GESIMA) on the left side and by the C-band model (CMOD4) from ERS-1 SAR data on the right side. The solid lines represent isotachs in m/s.

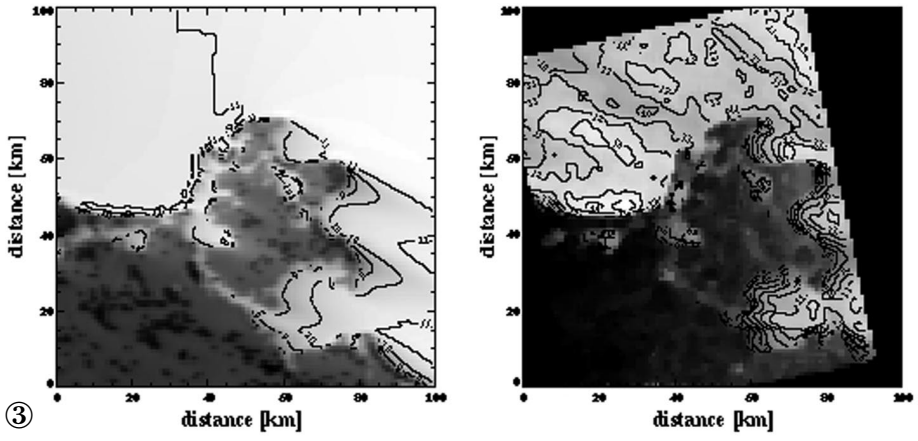

③

Conclusion

Application of the C-band models CMOD4 and CMOD IFR2 to ERS SAR images result in valuable information on mesoscale wind fields over the ocean. If wind streaks appear in ERS SAR

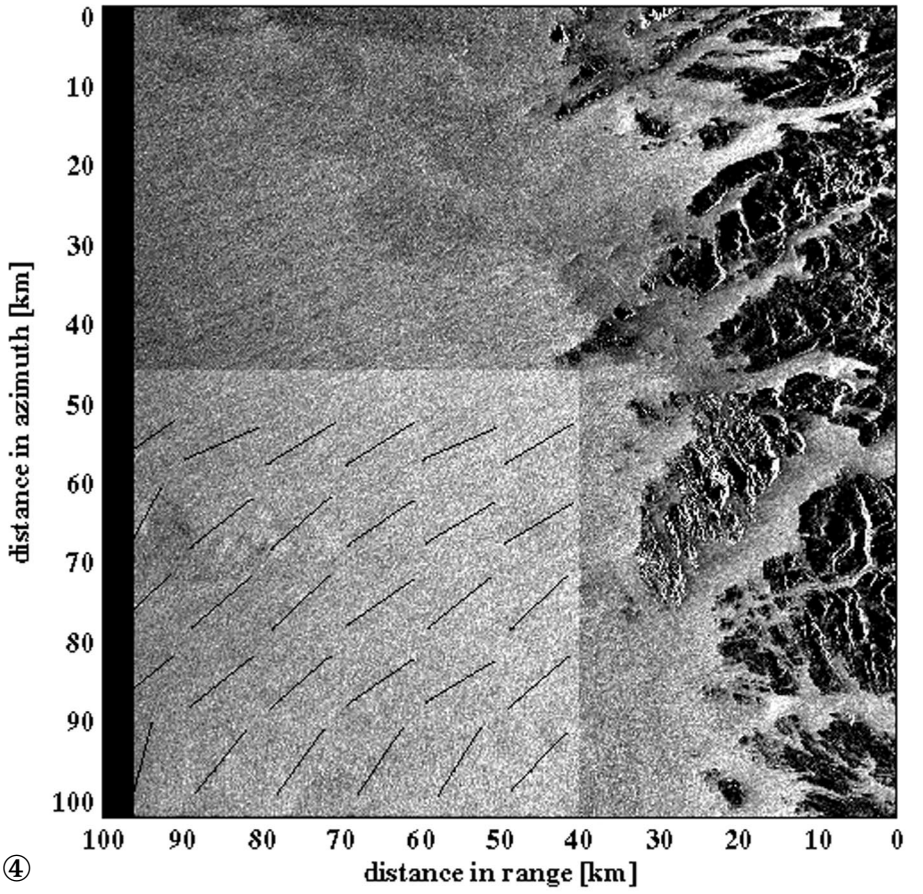

④

ERS-1 SAR image of the west coast of the Shetland Islands, taken on 1 Dec. 1992, at 10:28 UTC. The highlighted area was taken to investigate the wind variability. The superimposed solid lines represent the wind direction as computed from the wind streaks.

images, wind direction can be retrieved with an 180° ambiguity which can be removed if wind shadowing is visible. Comparisons of SAR-derived wind speeds to results of the mesoscale model GESIMA showed finer details of wind speeds in the ERS SAR data, resulting in richer information in comparison to the model results. The spatial wind variation over the ocean surface with ERS SAR images showed a distinct reduction of spectral density with an increasing wave number and a slope according to $k^{-5/3}$.

The spectral density versus wave number is plotted in log-log coordinates. The spectral density was computed from the wind-speed spectrum. The corresponding wavelengths are plotted under the wave number axis.

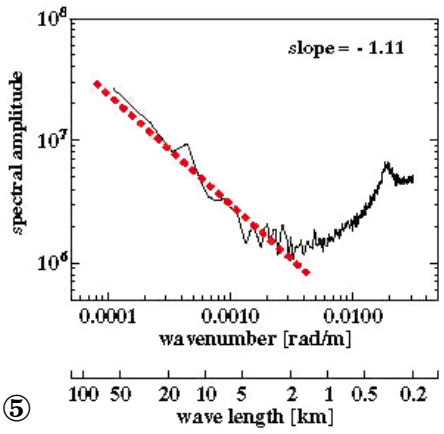

⑤

References

Alpers WR & B Brümmer, Atmospheric boundary layer rolls observed by the synthetic aperture radar aboard the ERS-1 satellite, *JGR* **99**, 12613-12621, 1994.

Chapron B, T Elfouhaily & V Kerbaol, A SAR speckle wind algorithm, in *Proc. 2nd ERS-1 Workshop,* pp. 5-40, Ifremer, Brest, France, 1994.

Gage KS & GD Nastrom, Theoretical interpretation of atmospheric wavenumber spectra of wind and temperature observed by commercial aircraft during GASP, *J.Atmos.Sci.* **43**:7, 729-740, April 1996.

Horstmann J, Untersuchung zur Windgeschwindigkeitsbestimmung aus dem Radar mit synthetischer Apertur an Bord der ERS-1/2-Satelliten, *external GKSS report, GKSS 97/E/55, ISSN 0344-9629*, 1997.

Kaimal JC, JC Wyngaard, Y Izumi & OR Cote, Spectral characteristics of surface layer turbulence, *Q.J. Roy.Meteor. Soc.* **98**, 563-589, 1972.

Kapitza H & DP Eppel, The non-hydrostatic mesoscale model GESIMA, I - Dynamical equations and tests, *Contrib. Atmos.Phys.* **65** (2), 129-146, May 1992.

Korsbakken E, Quantitative wind field retrievals from ERS SAR images, YGT report, *ESA ESTEC, Printed by TIDC Repro.*, 1996.

Laur H, P Bally, P Meadows, J Sanchez, B Schaettler & E Lopinto, Derivation of the backscattering coefficient s_0 in ESA ERS SAR PRI products, *Tech. Note ES-TN-RS-PM-HL09*, issue 2, rev.4, 41 p., ESA, Frascati, Italy, May 1997.

Lehner S, J Horstmann, W Koch & W Rosenthal, Mesoscale wind measurements using recalibrated ERS SAR images, *JGR*, in press.

Quilfen Y & A Bentamy, Calibration/ Validation of ERS-1 scatterometer precision products, *Proc. IGARSS 1994*,

Scoon A, IS Robinson, & PJ Meadows, Demonstration of an improved calibration scheme for ERS-1 SAR imagery using a scatterometer wind model, *Int.J. Remote Sens.* **17** (2), 413-418, 1996.

Stoffelen A & D Anderson, Scatterometer data interpretation: Estimation and validation of the transfer function CMOD4, *JGR* **102**, 5767-5780, 1997.

Vachon P & FW Dobson, Validation of wind vector retrieval from ERS-1 SAR images over the ocean, *The Global Atm. & Ocean Syst.,* **5**, 177-187, 1996.

Wakerman CC, CL Rufenach, R Schuchman, J.A. Johannessen & K. Davidson, Wind vector retrieval using ERS-1 synthetic aperture radar imagery, *JGR* **34**, 1343-1352, 1996.

Acknowledgements
This work was supported by the Bundesministerium für Bildung und Forschung (BMBF) under contract No. 03F0165C. The ERS SAR images were kindly provided by ESA as part of the SARPAK project, under grant AO02.D113.